The object of this study was $LiFePO_4$/C cathode material synthesized using a ferronickel-derived $FePO_4$ precursor, with the main focus is the effect of carbon addition on phase formation and electrochemical performance. The problem was how carbon addition affects olivine $LiFePO_4$ phase formation, impurity suppression, microstructure, and electrochemical performance when a non-commercial ferronickel-derived iron precursor is used. The precursor was mixed with LiOH as a lithium source and varying amounts of carbon from Super P: 5 wt.%, 7 wt.%, and 9 wt.%. Carbon addition influenced the formation of olivine $LiFePO_4$. At 7 wt.% LFP/C, the diffraction pattern was dominated by the $LiFePO_4$ phase, around 99.60% based on Rietveld refinement. The absence of detectable Ni by EDX suggests that Ni carryover from the ferronickel-derived precursor was minimized. The results suggest that ferronickel-derived $FePO_4$ can be used as a precursor for $LiFePO_4$/C synthesis, and carbon addition promotes phase development with 7 wt.% as the optimum composition. The results can be practically used as a basis for developing value-added $LiFePO_4$/C cathode materials from ferronickel-derived iron resources under controlled synthesis conditions, particularly when the $FePO_4$ precursor purity is maintained, Super P carbon is used in the range of 5–9 wt.%, and the material is processed by ball milling, preheating at 300°C, and calcination at 650°C under an argon atmosphere. The 7 wt.% LFP/C sample had a specific capacity of 140 mAh g^{-1} at 0.1 C, but electrochemical performance still requires optimization due to particle interconnection and agglomeration. EIS data show that 7 wt.% carbon is the most favorable composition in terms of charge-transfer resistance (34.91 Ω) and conductivity (2.79×10^{-4} S/cm), while 9 wt.% carbon provided the best lithium-ion diffusion characteristics (1.96×10^{-13} cm^2 s^{-1}). These results indicate that ferronickel-derived iron resources have strong potential to be converted into value-added battery cathode materials

Keywords: ***$LiFePO_4$, ferronickel-derived $FePO_4$, carbon addition, phase formation, cathode materials***

UDC 544.6:621.355.4
DOI: 10.15587/1729-4061.2026.365363

IDENTIFICATION THE IMPACT OF CARBON ADDITION ON PHASE FORMATION AND ELECTROCHEMICAL PERFORMANCE OF LIFEPO$_4$/C SYNTHESIZED FROM FERRONICKEL-DERIVED FEPO$_4$

Vita Astini
Student*
ORCID: https://orcid.org/0000-0002-1499-8364
Anne Zulfia Syahrial
Corresponding Author
Professor*
E-mail: anne.zulfia@ui.ac.id
ORCID: https://orcid.org/0009-0005-3949-8437
Achmad Subhan
Research Center for Advanced Materials
National Research and Innovation Agency
Tangerang Selatan, Indonesia, 15314
ORCID: https://orcid.org/0000-0002-0774-9220
Johny Wahyuadi Mudaryoto Soedarsono
Professor*
ORCID: https://orcid.org/0000-0001-6051-2866
*Department of Metallurgy & Materials Engineering
Universitas Indonesia
Margonda Raya str., Depok, Indonesia, 16424

Received 20.03.2026
Received in revised form 02.06.2026
Accepted date 11.06.2026
Published date 30.06.20226

How to Cite: *Astini, V., Syahrial, A. Z., Subhan, A., Mudaryoto Soedarsono, J. W. (2026). Identification the impact of carbon addition on phase formation and electrochemical performance of $LiFePO_4$/C synthesized from ferronickel-derived $FePO_4$. Eastern-European Journal of Enterprise Technologies, 3 (12 (141)), 36–47. https://doi.org/10.15587/1729-4061.2026.365363*

1. Introduction

Lithium iron phosphate ($LiFePO_4$, LFP) is known as one of the critical cathode materials for lithium-ion batteries due to its high thermal stability, long cycle life, inherent safety, and low cost. Special attention is devoted to achieving higher power and energy densities, along with enhancing safety and reducing cost [1]. $LiFePO_4$ is of great interest due to its fast-charging capability and high stability regarding its thermal resistance and chemical reactivity [2]. These properties make LFP attractive for electric vehicle (EV) and stationary energy storage, even though its practical performance is strongly dependent on precursor quality, electronic conductivity (EC), and synthesis route. Since the cathode serves as a central component of LIBs, the overall cell performance is significantly affected by the chemical and physical properties of the cathode [3].

Despite these advantages, the practical application is limited by the material's intrinsically low electronic conductivity and lithium-ion diffusion coefficient, which restrict its rate capability [4]. The low conductivity of lithium iron phosphate and the slow diffusion rate of lithium ions also restricted the development of lithium iron phosphate in the power battery industry [5].

The quality of the Fe precursor is particularly important because it can influence phase formation, particle growth, impurity behavior, and the final electrochemical performance of $LiFePO_4$/C. Several alternative Fe-based precursors have been explored for LFP/C synthesis. For example is LiFePO4/C composites synthesized using Fe-P waste slag from the industrial production of yellow phosphorus with

an initial discharge capacity of 150 mAh/g at 0.1 C [6]. It is also reported that the synthesis of LFP/C from cold roll Fe_2O_3 showed an initial discharge capacity of 163 mAh/g at 0.1 C [7]. These studies show that non-commercial Fe sources can be converted into LFP/C cathode materials, although their performance remains highly dependent on precursor purity, synthesis route, and carbon modification.

For Indonesia, this direction is especially relevant from both scientific and industrial perspectives. Recent analyses of Indonesia's nickel downstreaming pathway show that the country has made major progress in processing nickel domestically, but the transition from lower-value downstream products toward more advanced battery materials remains uneven [8]. At present, downstream success has been stronger in stainless steel-oriented pathways than in higher-value battery-material chains, which means that converting domestic ferronickel-related resources into battery precursor materials could contribute to value addition and broader participation in battery supply chains. From this perspective, developing $FePO_4$ and LFP from ferronickel-derived local content is not only a materials synthesis problem but also part of a wider resource valorization strategy.

Therefore, studies that are devoted to understanding the effect of carbon addition on the synthesis of $LiFePO_4$/C from a non-commercial ferronickel-derived $FePO_4$ precursor are of scientific relevance. The use of ferronickel-derived $FePO_4$ provides an opportunity to explore the utilization of ferronickel-related materials in $LiFePO_4$ production.

2. Literature review and problem statement

Among the many factors that control lithium iron phosphate quality, the properties of the $FePO_4$ precursor are crucial. The characteristics of iron phosphate precursors strongly influence the performance of $LiFePO_4$ cathodes [9]. Similarly, $LiFePO_4$/C synthesized from monoclinic $FePO_4$ exhibited a well-developed carbon-coated structure, uniformly distributed primary particles, high crystallinity, and excellent electrochemical performance [10]. The $FePO_4$ route is one of the most controllable and promising methods for $LiFePO_4$ synthesis. In the preparation of lithium iron phosphate by carbothermic reduction, iron phosphate ($FePO_4$) as one of the raw materials is closely related to the electrochemical performance of lithium iron phosphate, and its particle agglomeration, morphology, crystallinity, and other characteristics will affect lithium iron phosphate [11]. There is an unresolved issue regarding how non-commercial $FePO_4$ derived from metallurgical resources behaves during conversion into $LiFePO_4$/C, because most reported preparation routes still rely on chemical reagents or commercial precursors, and only a limited number of studies have considered ferronickel-derived iron resources as $FePO_4$ precursors.

Increasing the added value of iron and mineral resources is important for Indonesia. The converted Fe recovered from laterite nickel tailings into battery-grade $FePO_4$ and subsequently synthesized high-performance $LiFePO_4$ was reported [12]. A related study, iron obtained from laterite nickel ore was used to prepare $LiFePO_4$/C [13]. This study is relevant because it shows the possibility of using nickel-related mineral resources for cathode material synthesis. Although their work used laterite-derived Fe_2O_3, but not ferronickel-derived $FePO_4$. Therefore, it is still necessary to study ferronickel-derived $FePO_4$ as an alternative precursor for $LiFePO_4$/C cathode materials.

In addition to precursor quality, carbon addition is also important in $LiFePO_4$/C synthesis. Carbon coating has been reported to improve the electronic conductivity and electrochemical performance of $LiFePO_4$ cathodes [14]. However, its effect is not always the same because it depends on the precursor, carbon source, and synthesis condition. The characteristics of $FePO_4$ precursors also affect the phase formation and electrochemical performance of $LiFePO_4$/C [15]. However, their study used controlled $FePO_4$ precursors, while $FePO_4$ obtained from ferronickel may have different characteristics. Carbon content and carbonization temperature influence the quality of carbon coating and the performance of $LiFePO_4$/C [16]. However, the suitable carbon content may be different when a ferronickel-derived $FePO_4$ precursor is used. The impurities in $FePO_4$ raw materials can affect the structure and electrochemical properties of $LiFePO_4$ cathodes. Mn^{2+} doping leads to a significant decline in the rate performance of LFP [17]. This is important because ferronickel-derived $FePO_4$ may carry impurity risks, especially from Ni, Mn, and Co.

$FePO_4$ precursor quality, impurity control, and carbon addition are important factors in $LiFePO_4$/C synthesis. However, the conversion of ferronickel-derived $FePO_4$ into $LiFePO_4$/C has not been clearly discussed, especially in relation to phase formation, elemental purity, particle morphology, and electrochemical performance. This gap may occur because ferronickel-derived solutions contain more than one metal ion, so Fe separation, impurity control, and carbon optimization become more difficult. Therefore, it is necessary to study the effect of carbon addition on the phase formation, impurity behavior, microstructure, and electrochemical performance of $LiFePO_4$/C synthesized from ferronickel-derived $FePO_4$.

3. The aim and objectives of the study

The aim of the study is to identifying the effect of carbon addition on the phase formation, impurity behavior, microstructural characteristics, and electrochemical performance of $LiFePO_4$/C synthesized from a ferronickel-derived $FePO_4$ precursor. This will make it possible to find the optimum carbon content and makes ferronickel-derived $FePO_4$ a viable alternative for battery cathode materials.

To achieve this aim, the following objectives were accomplished:

– to evaluate the effect of carbon addition on olivine $LiFePO_4$ phase formation and secondary phase development;

– to investigate the effect of carbon addition on the microstructural characteristics of $LiFePO_4$/C materials;

– to evaluate the surface area, total pore volume, and average diameter pore based on N_2 adsorption–desorption analysis;

– to evaluate the electrochemical performance of $LiFePO_4$/C cathodes using CV, EIS, and galvanostatic charge-discharge tests to achieve the optimum carbon content.

4. Materials and methods

The object of this study was $LiFePO_4$/C cathode material synthesized using a ferronickel-derived $FePO_4$ precursor, with the main focus is the effect of carbon addition on phase formation and electrochemical performance. The main hypothesis of this study was that iron dissolved from ferronickel can be converted into $FePO_4$ and subsequently used as a

precursor for $LiFePO_4$/C synthesis, while carbon addition affects phase formation, impurity behavior, and microstructural characteristics of the final product. This study assumed that Fe recovered from ferronickel after electrodissolution (Fig. 1, *a*) and precipitation (Fig. 1, *b*) could act as the main Fe source for $FePO_4$ formation (Fig 1, *c*). For simplification, the effects of carbon addition were evaluated mainly through phase formation, elemental distribution, and electrochemical performance.

Ferronickel from Southeast Sulawesi [18, 19], Indonesia, was used as the iron source for preparing the $FePO_4$ precursor. Lithium hydroxide (LiOH) and ethanol were purchased from Merck, while Super P, PVDF, NMP, lithium foil, separator, Al foil, spacer, spring, and CR2032 coin-cell cases were purchased from Sigma-Aldrich.

$FePO_4$ precipitate was prepared from an electrolyte (Fig. 1, *a*) with dissolved metal ions produced by electrodissolving ferronickel. Hydrochloric acid served as the electrolyte, as described in earlier studies on ferronickel electrolysis [18, 19]. After precipitation, the $FePO_4$ was dried at 105°C for 4 hours (Fig. 1, *b*) and then sintered at 500°C for 3 hours in MTI KSL-1200X furnace to remove both adsorbed and structural water (Fig. 1, *c*). This process produced a stable, anhydrous $FePO_4$ precursor suitable for later $LiFePO_4$/C synthesis.

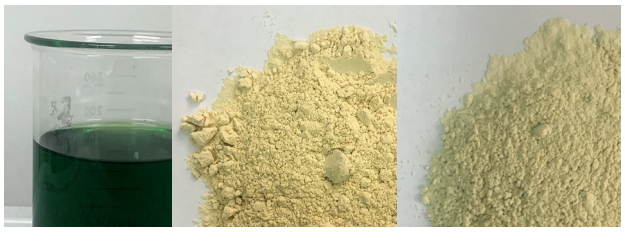

a *b* *c*

Fig. 1. $FePO_4$ preparation: *a* — electrolyte with dissolved metal; *b* — dried $FePO_4$; *c* — sintered $FePO_4$

$LiFePO_4$/C was prepared by mixing ferronickel-derived $FePO_4$ with LiOH as the lithium source, using 5% excess LiOH to compensate for lithium loss during heat treatment. The main experimental variable was the amount of carbon added during $LiFePO_4$/C synthesis. The carbon addition variables are 5 wt.%, 7 wt.%, and 9 wt.%. The precursor mixture was planetary ball-milled at 300 rpm for 2 h using Deco 400-800-4256. After ball mill, the sample preheated at 300°C for 3 h, and subsequently calcined at 650°C for 10 h to obtain olivine $LiFePO_4$/C (Fig. 2) using tube furnace MTI OFT-1200X. The heat treatment was carried out under an argon atmosphere. The product was then naturally cooled to room temperature and ground up to 400 mesh before characterization.

The synthesized $LiFePO_4$/C samples (Fig. 2) were characterized using several analytical techniques. The crystal structure was analyzed by X-ray diffraction (XRD, PANalytical X'Pert Pro), while the morphology and elemental distribution were examined using scanning electron microscopy equipped with energy-dispersive X-ray spectroscopy. A mixture of $LiFePO_4$/C, Super P conductive additive, and polyvinylidene fluoride (PVDF) binder in N-methyl-2-pyrolidone (NMP) at an 80:10:10 weight ratio formed the cathode slurry. The slurry was homogenized and coated onto aluminum foil using the doctor blade technique. After drying at 60°C for 2 hours, the coated foil was pressed to enhance wettability and electrical contact, then punched into circular disks.

Fig. 2. Powder of synthesized $LiFePO_4$/C

CR2032 coin cells were assembled in an argon-filled glovebox, with the prepared electrode as the working electrode. Lithium metal foil served as the counter and reference electrode, and a microporous polypropylene membrane as the separator and $LiPF_6$ as electrolyte.

The electrochemical properties of the synthesized $LiFePO_4$/C were evaluated by Wonatech cyclic voltammetry (CV), Hioki electrochemical impedance spectroscopy (EIS), and Neware galvanostatic charge–discharge (GCD) test. CR2032 coin cells were assembled with lithium metal as the counter/reference electrode, a microporous separator, and 1 M $LiPF_6$ in EC/DMC as the electrolyte. CV measurements were performed in the voltage range of 2.0–4.5 V at a scan rate of 0.1 mV s^{-1}. EIS was carried out over the frequency range of 0.1 Hz to 50 kHz with an applied amplitude of 5 mV. GCD measurements were conducted at various rates of 0.1C, 0.2C, 0.5C, 1C, and 2C to evaluate the specific capacity and rate capability of the $LiFePO_4$/C electrodes.

5. Results of $LiFePO_4$/C synthesis and battery assembly with different carbon contents

5. 1. Effect of carbon addition on olivine $LiFePO_4$ phase formation

Fig. 3 shows the XRD patterns of $LiFePO_4$/C samples prepared with different carbon contents of 5, 7, and 9 wt.%. The samples were synthesized from ferronickel-derived $FePO_4$ and heat-treated by preheating at 300°C for 3 h followed by calcination at 650°C for 10 h. The XRD patterns show the formation of $LiFePO_4$ derived from a $FePO_4$ precursor. Although $LiFePO_4$/C is formed as the major phase in all compositions, the secondary phases were also detected in the sample with different carbon content. This indicates that the carbon content affected to the phase formation of olivine $LiFePO_4$/C.

The diffraction pattern of the 5 wt.% carbon sample displays the crystalline $LiFePO_4$ olivine reflections, suggesting the $FePO_4$ reacted with lithium source during heat treatment. However, additional reflections corresponding to $LiFe_2P_2O_7$ were still observed, showing that the transformation into single-phase $LiFePO_4$ was incomplete. Based on Rietveld refinement, the sample with a 5 wt.% carbon composition had a phase purity of 93.10%, indicating a predominantly single-phase material with a minor secondary phase. This result suggests that 5 wt.% carbon was insufficient to provide a favorable reaction environment for complete phase transformation during heat treatment. Fig. 4 shows the enlarged X-ray diffraction patterns highlighting secondary phosphate phases in $LiFePO_4$/C.

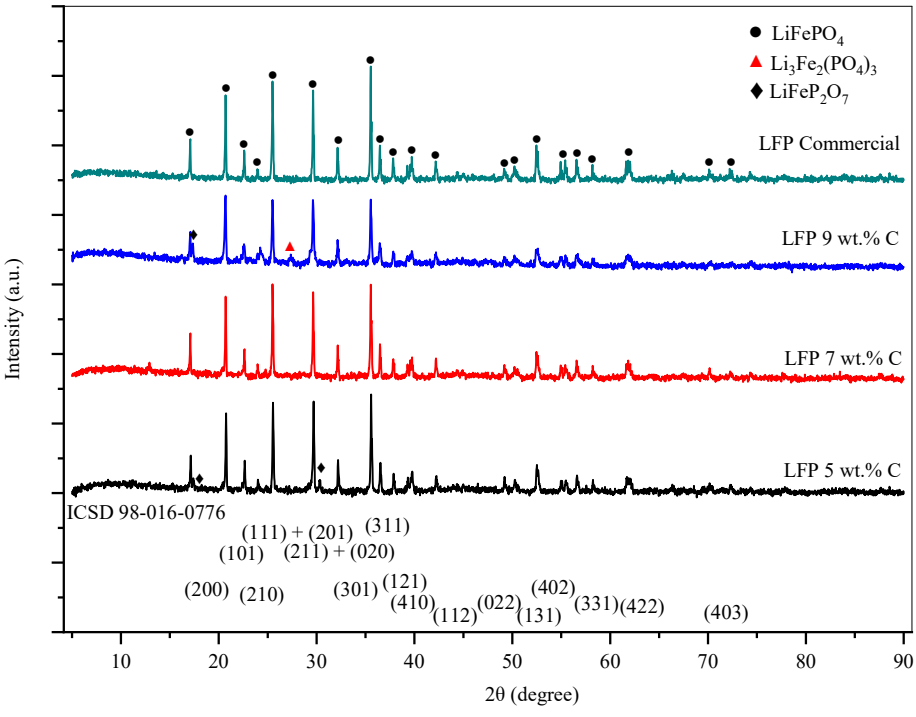

Fig. 3. X-ray diffraction patterns of $LiFePO_4$/C samples prepared with different carbon contents of 5, 7, and 9 wt.% from ferronickel-derived $FePO_4$ after preheating at 300°C for 3 h and calcination at 650°C for 10 h

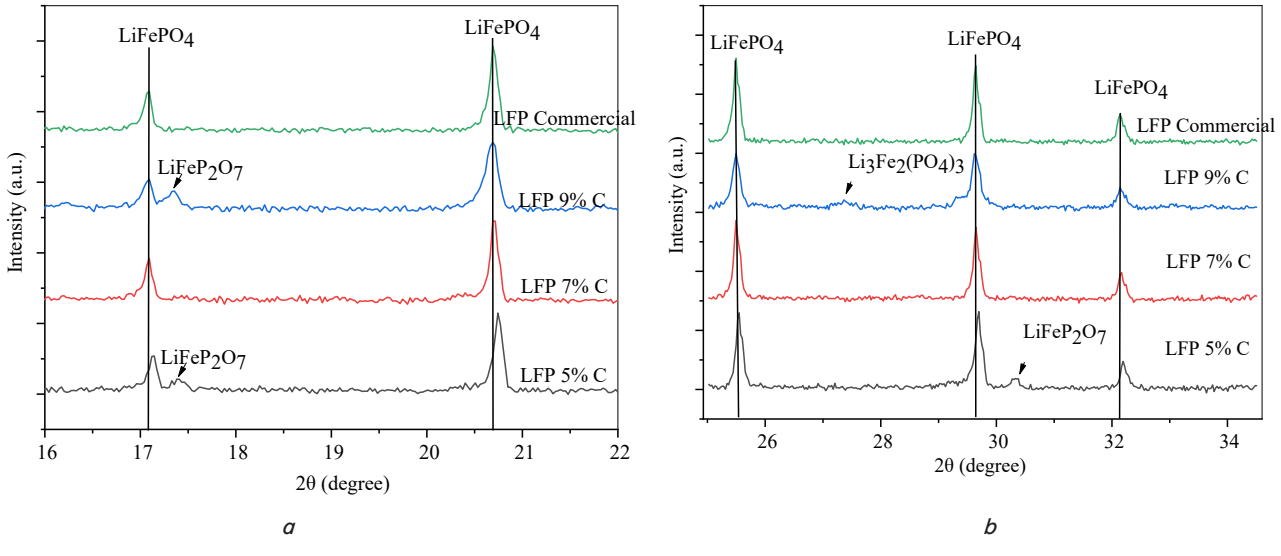

Fig. 4. Enlarged X-ray diffraction patterns highlighting secondary phosphate phases in $LiFePO_4$/C samples prepared with different carbon contents: *a* – 2θ = 16°–22°; *b* – 2θ = 25°–34.5°

The 7 wt.% carbon addition sample showed a $LiFePO_4$ diffraction pattern most similar to commercial $LiFePO_4$, with the main reflections of LFP/C and no secondary phase peaks. Based on Rietveld refinement, the 7 wt.% carbon sample has the highest phase purity of 99.60%, while the 9 wt.% carbon sample has a lower phase purity of 80.40%. The 7 wt.% sample indicates complete phase formation, and the carbon addition supports optimal carbon content for $LiFePO_4$ formation under current conditions. The carbon content at this level supports a complete reaction mode of the ferronickel-derived $FePO_4$ precursor phase with LiOH, maintaining optimal ratios in reaction balance over thermal treatment. The higher phase purity at 7 wt.% C suggest that proper carbon content can helps provide reaction environment, allowing the precursor to convert to the olivine $LiFePO_4$ structure more efficiently [9]. Fig. 4 highlights the secondary phases formed during $LiFePO_4$ synthesis. In the 5 wt.% carbon sample, secondary $LiFeP_2O_4$ peaks were observed at $2\theta = 17.38°$ and 30.03°. In the 9 wt.% carbon sample, $LiFeP_2O_4$ was detected at $2\theta = 17.35°$, while $Li_3Fe_2(PO_4)_3$ was observed at $2\theta = 30.03°$.

5. 2. Microstructural characteristics and Energy Dispersive of X-ray Spectroscopy analysis

SEM images in Fig. 5 reveal the differences in particle aggregation and surface morphology among the $LiFePO_4$/C samples with different carbon contents. The 5 wt.% carbon sample consisted of large and compact

agglomerates with interconnected particles, dense packing, and relatively smooth surfaces (Fig. 5, *a*). This morphology suggests that the carbon level was insufficient to effectively suppress particle coalescence during heat treatment.

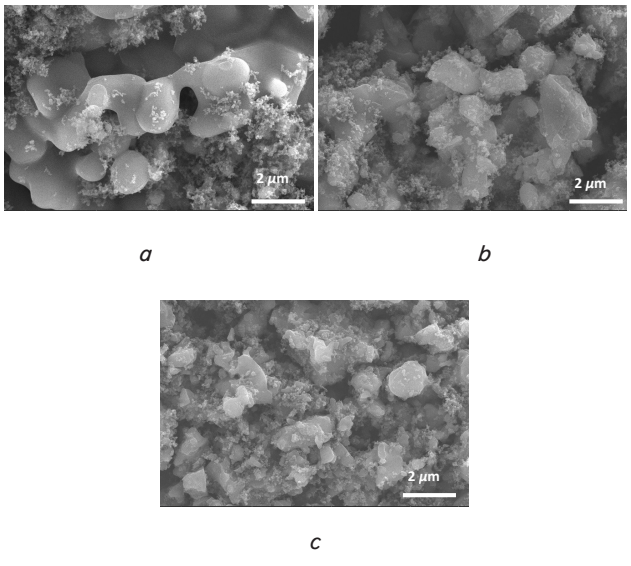

a *b*

c

Fig. 5. Scanning electron microscope (SEM) images of $LiFePO_4/C$ with different carbon contents and magnifications: *a* – 5 wt.%; *b* – 7 wt.%; *c* – 9 wt.%, observed at 10,000× magnifications

Low carbon content was unable prevent the particles from agglomeration in the calcination step [20]. Such agglomerated particles are expected to have worse electrochemical performance. As a consequence, the active particles became closely packed, which is unfavorable for electrolyte penetration and lithium-ion transport [21].

A compact morphology disrupts a continuous conductive network, reducing electrochemical utilization. The 7 wt.% carbon sample (Fig. 5, *b*) exhibited a less compact aggregate structure than the 5 wt.% sample, with more open interparticle spaces and a rougher surface texture. Although agglomeration was still observed, the particles appeared more evenly arranged, suggesting a better balance between particle connectivity and structural accessibility [13].

The morphology suggests that carbon distribution may not be fully uniform, which could affect interparticle electronic contact. The 9 wt.% (Fig. 5, *c*) carbon sample exhibits a finer, fragmented morphology and less compact particle packing. Compared with the 5 wt.% sample, the structure appears more porous and more accessible. However, excessive carbon may also reduce effective interfacial contact between $LiFePO_4$ particles and the electron-transporting network if carbon distribution becomes non-uniform and segregates.

Fig. 6 shows the EDX mapping for Fe (green), P (yellow) and O (red) on the $LiFePO_4/C$. The mapping results show that Fe, P, and O are distributed throughout the particle regions for all samples, indicating the formation of phosphate-based particles with relatively homogeneous elemental distribution. This indicates that the constituent elements were relatively homogeneously distributed after $LiFePO_4/C$ synthesis.

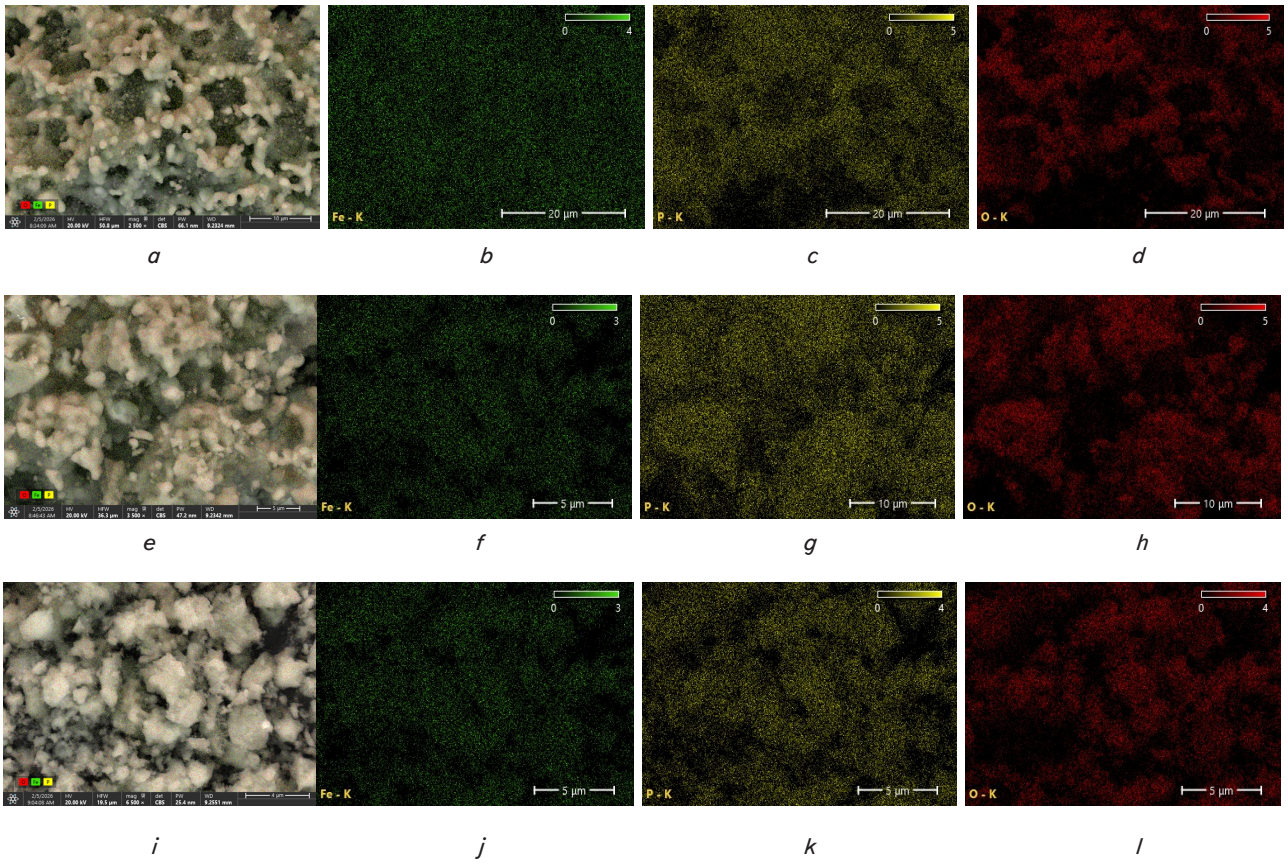

a *b* *c* *d*

e *f* *g* *h*

i *j* *k* *l*

Fig. 6. Energy-dispersive X-ray spectroscopy (EDS) elemental mapping of $LiFePO_4/C$ with different carbon contents: *a*–*d* – 5 wt.% carbon; *e*–*h* – 7 wt.% carbon; *i*–*l* – 9 wt.% carbon correspond to the distribution of all detected elements, Fe, P, and O, respectively

Fig. 6, *a–l*, show with various carbon contents, there is no segregation of Fe, P, and O. All samples exhibit the presence of Fe, P, and O, indicating the formation of phosphate-based materials. The elements are well distributed to the particles, even from the Morphology in Fig. 5 shows that the particles agglomerate. This indicates that the variation in carbon content did not strongly affect the spatial distribution of the main constituent elements.

Fig. 7 presents the EDX spectra of the $LiFePO_4$/C samples. The detected elements were mainly Fe, P, and O, with relative atomic ratios varying depending on carbon content. No additional elements were detected within the detection limit of EDX analysis. The Fe:P ratios were approximately 1:0.87, 1:0.92, and 1:0.99 for the 5, 7, and 9 wt.% carbon samples, respectively. The Fe:P ratio became closer to the nominal stoichiometric ratio with increasing carbon content, although EDX provides only semi-quantitative elemental information.

Based on Fig. 7, *a–c*, the detected elements were mainly Fe, P, and O, and C with relative atomic ratios varying depending on the carbon content. There is a peak of C that relates to the carbon content, because the peak increases with increasing carbon content. The P peak also increases with increasing carbon content. This relates to the EDX result, which shows that the sample with 9 wt.% (Fig. 7, *c*) has a higher stoichiometric Fe:P ratio that is 1:0.99.

5. 3. Surface area, total pore volume, and average diameter pore based on N_2 adsorption–desorption analysis

The N_2 adsorption-desorption isotherms of LFP/C samples with varying carbon contents (5, 7, and 9 wt.%) and the LFP commercial material are presented in Fig. 8. All samples exhibit mesoporous behavior, with adsorption volume rising gradually at low pressure and sharply near $P / P_0 = 1.0$.

Fig. 8 shows that the 9 wt.% carbon sample has the highest nitrogen adsorbed volume among the samples. This means that the 9 wt.% carbon sample has higher accessible porosity than the other samples. The 7 wt.% carbon sample shows a lower nitrogen adsorbed volume than the 9 wt.% sample, while the 5 wt.% carbon sample shows the lowest nitrogen adsorbed volume. This result is related to the SEM morphology in Fig. 5, *a*, where the 5 wt.% sample appears more agglomerated and compacted. This compact structure can reduce the accessible pores and lower the nitrogen adsorption volume.

The commercial sample has the highest adsorption volume, a surface area of 6.888 m^2/g, and the largest pore volume (Table 1). Among the synthesized materials, adsorption uptake increases with increasing carbon content, which is 9 wt.%, 7 wt.%, and 5 wt.% in sequence. Although higher carbon content increased the adsorption uptake and BET surface area, the electrochemical results show that textural improvement alone was insufficient to guarantee superior cathode performance.

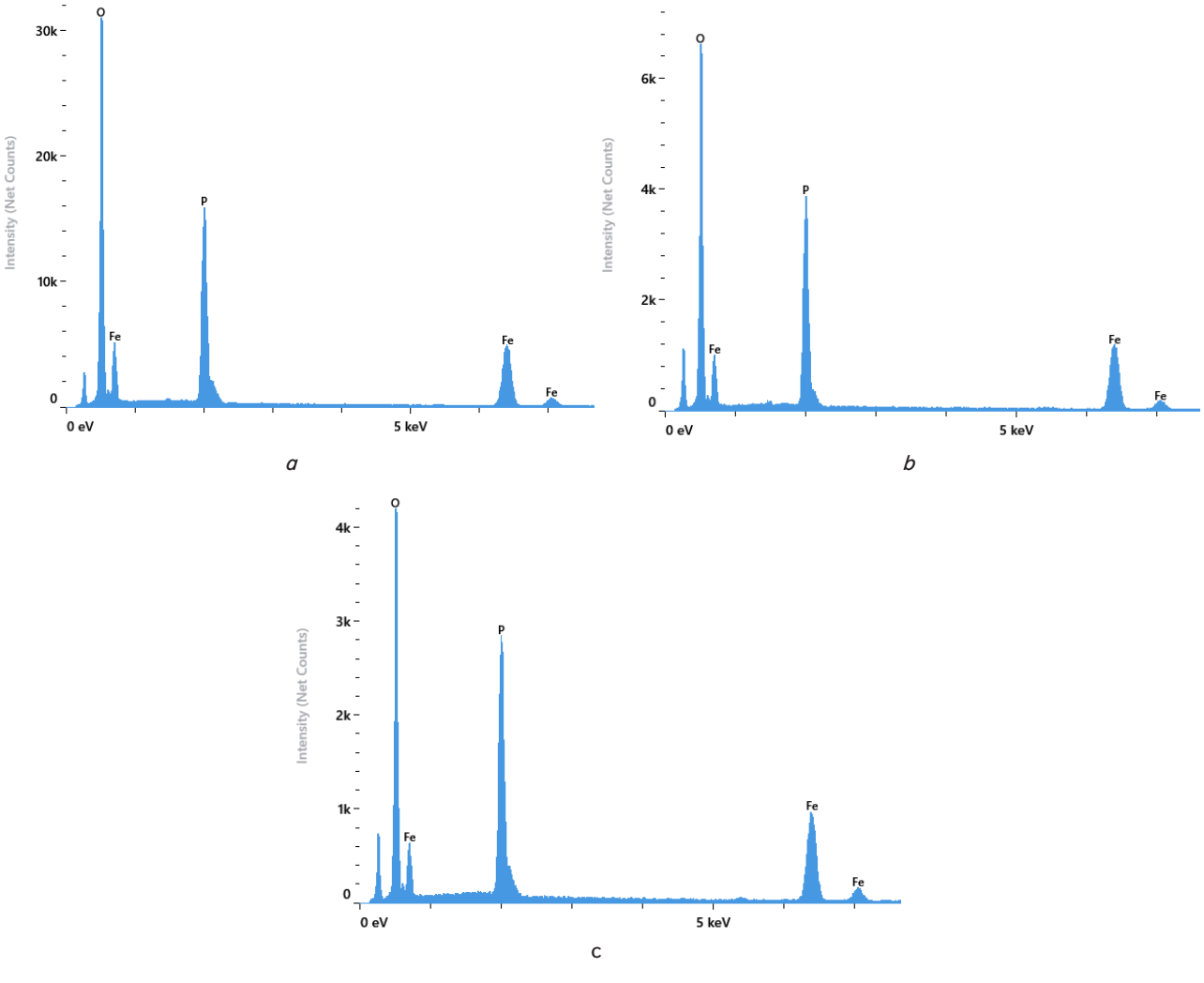

Fig. 7. Energy dispersive of X-ray spectroscopy mapping intensity of $LiFePO_4$/C with various carbon content *a* – 5 wt.%; *b* – 7 wt.%; *c* – 9 wt.%

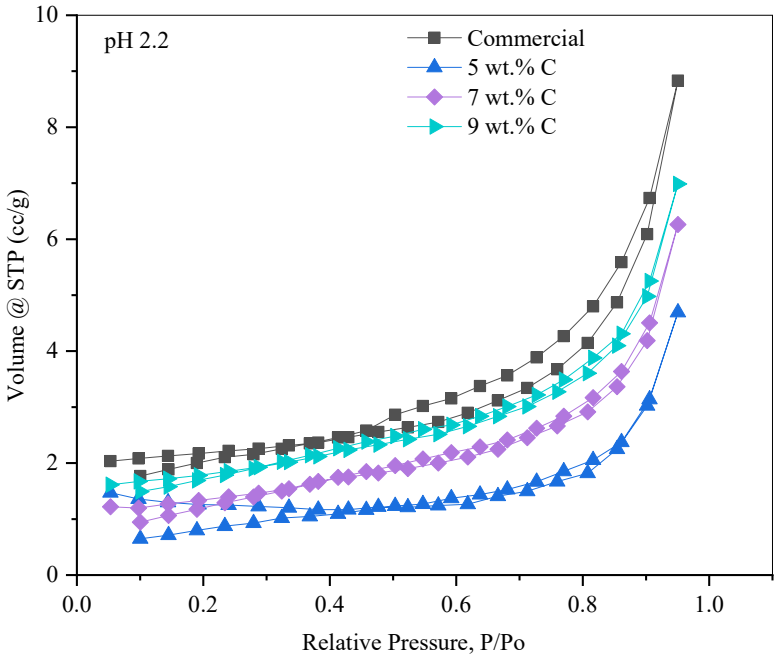

Fig. 8. The gas adsorption isotherms of the commercial and ferronickel-derived $LiFePO_4/C$ samples prepared with different carbon contents

Table 1

Textural properties of LFP/C samples and LFP commercial obtained from N_2 adsorption-desorption analysis

Sample	Carbon content			
	5 wt.%	7 wt.%	9 wt.%	Commercial
BET surface area (m^2/g)	3.651	4.513	5.913	6.888
Total pore volume (cm^3/g)	0.007256	0.009687	0.01081	0.01366
Average pore diameter (nm)	7.95	8.59	7.31	7.93
Pore Category	Mesoporous	Mesoporous	Mesoporous	Mesoporous

The 9 wt.% C sample, with a surface area of 5.913 m^2/g, has the highest adsorption uptake (Fig. 7), indicating improved pore accessibility and textural development. However, its electrochemical performance did not improve proportionally, possibly due to non-uniform carbon distribution or less effective electronic contact.

The 7 wt.% sample had a BET surface area of 4.513 m^2/g and total pore volume of 0.009687 cm^3/g, both higher than those of the 5 wt.% sample. It also exhibited the largest average pore diameter of approximately 8.59 nm, suggesting a more open mesoporous structure that may facilitate electrolyte penetration and Li^+ transport. In contrast, the 5 wt.% sample had the lowest surface area of 3.651 m^2/g and total pore volume of 0.007256 cm^3/g, indicating a relatively compact structure with limited accessible porosity. The average pore diameter (~7.95 nm) falls within the mesoporous range, suggesting that mesopores are present but their volume is limited. This compact morphology may restrict electrolyte penetration and Li^+ transport, potentially leading to lower electrochemical utilization.

5. 4. Electrochemical performance of $LiFePO_4/C$ cathodes

The electrochemical impedance spectroscopy results (Fig. 9) show a strong carbon content influence on the charge-transfer and ion-diffusion behavior of $LiFePO_4/C$ samples.

Fig. 9 shows the Nyquist plots of $LiFePO_4/C$ samples with different carbon contents. The 5 wt.% carbon sample has the highest impedance, marked by large Z′ and −Z″ values, indicating high charge-transfer resistance and poor electronic conduction. The 7 wt.% sample shows intermediate impedance, between the 5 wt.% and 9 wt.% samples.

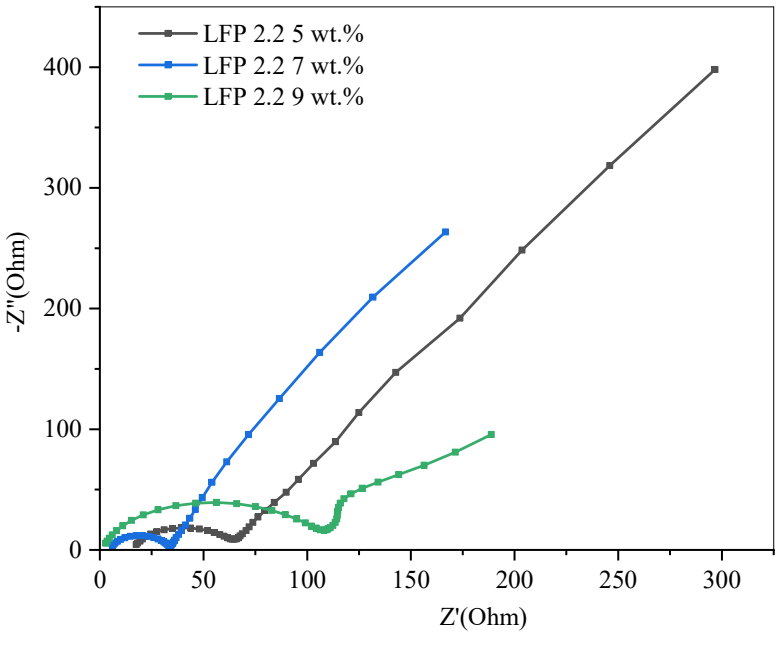

Fig. 9. Electrochemical impedance spectroscopy (EIS) Nyquist plots of different carbon content $LiFePO_4/C$ cathode materials

Although the 9 wt.% carbon sample shows the lowest impedance, this is not corresponding to the best overall electrode performance, because its phase purity is lower than that of the 7 wt.% carbon sample. The lower impedance of the 9 wt.% sample may be related to the higher carbon content, which improves conductivity. However, the 7 wt.% carbon sample provides a better balance between phase purity and electrochemical resistance. From Table 2, samples with 7 wt.% carbon exhibit the lowest charge-transfer resistance (34.91 Ω), the most favorable interfacial charge-transfer kinetics, and the highest conductivity (2.79×10^{-4}). This suggests that 7 wt.% carbon provides the most effective conductive network for electron transport.

In contrast, the 9 wt.% carbon sample shows the highest charge-transfer resistance (114.21 Ω) and the lowest conductivity (8.5×10^{-5}), indicating less favorable charge-transfer characteristics due to its higher carbon content. The 5 wt.% carbon sample has the lowest diffusion coefficient (2.44×10^{-14}) and the highest Warburg coefficient (178.72), confirming difficult ion transport.

Table 2

The EIS result analysis

Sample	Carbon content		
	5 wt.%	7 wt.%	9 wt.%
Rct (Ω)	68.80	34.91	114.21
D Li^+(cm^2 s^{-1})	2.44×10^{-14}	8.20×10^{-14}	1.96×10^{-13}
Warburg coefficient (Ω $s^{-1/2}$)	178.72	97.62	63.07
Conductivity (S/cm)	1.42×10^{-4}	2.79×10^{-4}	8.50×10^{-5}

The CV results in Fig. 10 indicate that the electrochemical reversibility and redox kinetics of $LiFePO_4$/C were strongly affected by carbon content. The 7 wt.% carbon sample exhibited the highest peak current, indicating enhanced electrochemical activity and improved redox kinetics. The peak separation (Δep) values were estimated to be approximately 0.27 V, approximately 0.27 V, and approximately 0.24 V for the 5 wt.%, 7 wt.%, and 9 wt.% samples, respectively. At 7 wt.%, the anodic peak is 3.57 V and the cathodic peak is 3.30 V, with a ΔEp of approximately 0.27. The peak separation (Δep) of 0.27 V for the 7 wt.% sample falls within the typical range for $LiFePO_4$-based cathodes, indicating moderate polarization and relatively fast electrochemical kinetics.

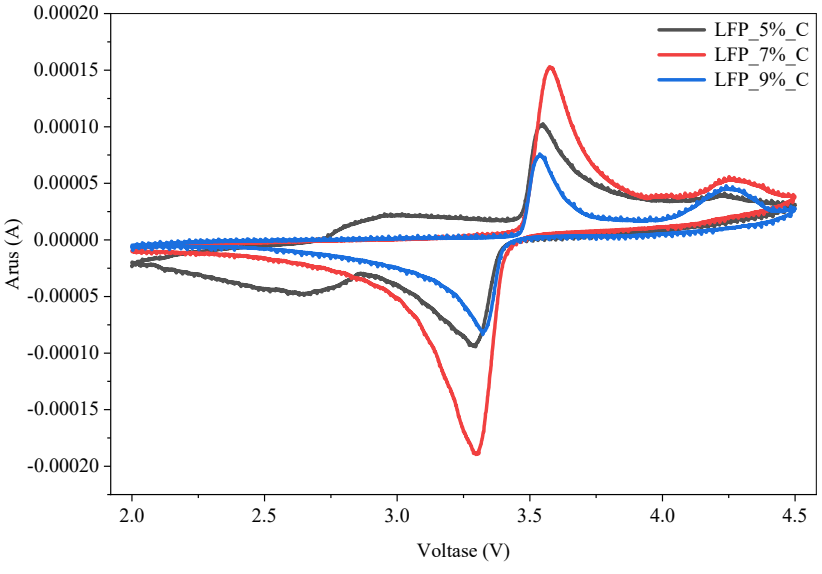

Fig. 10. Cyclic voltammetry (CV) curves of different carbon content $LiFePO_4$/C cathode materials measured in the voltage range of 2.0–4.5 V vs. Li/Li^+

The 5% carbon sample appears constrained by a lack of conductive support, whereas the 9 wt. % carbon sample shows the lowest peak current, which is attributed to the combined effects of excessive carbon and the formation of a secondary phase. These results confirm that optimizing, rather than maximizing, carbon content is essential for achieving balanced phase formation and electrochemical kinetics in ferronickel-derived $LiFePO_4$/C.

Fig. 11 shows the rate capability of ferronickel-derived $LiFePO_4$/C samples with varying carbon content. The 7 wt.% carbon sample shows the highest specific capacity, reaching about 140 mAh g^{-1}, followed by the 9 wt.% with 113 mAh g^{-1} and the 5 wt.% with 68 mAh g^{-1}. The 7 wt.% carbon sample had a higher capacity than the other samples at all rate stages, due to superior electrochemical utilization and better rate capability.

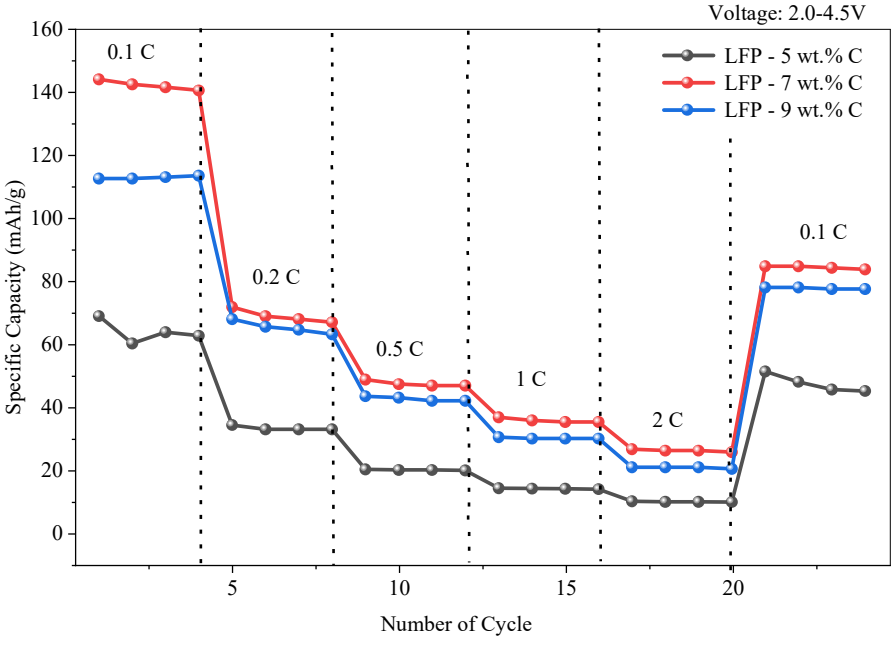

Fig. 11. Rate capability performance of $LiFePO_4$/C cathode materials with different carbon contents at various C-rates in the voltage range of 2.0–4.5 V

The 9 wt.% sample falls in the middle, while the 5 wt.% sample delivers the lowest capacity, likely due to insufficient conductivity and compact particle morphology. The 7 wt.% sample recovers most, balancing charge-transfer kinetics, conductivity, and lithium-ion transport. CV and EIS analyses confirm this, showing the 7 wt.% sample with the highest peak current, lowest charge-transfer resistance, and highest conductivity.

6. Discussion the effect of carbon addition on $LiFePO_4$ phase formation from Ferronickel-derived $FePO_4$

The results obtained in this study can be explained by the combined effect of carbon content on phase formation, particle morphology, and charge-transfer behavior. As shown in Fig. 3, 4, the XRD results show that phase purity depended on carbon content. The 7 wt.% sample shows an LFP peak and reached 99.60% based on Rietveld refinement results. The 5 wt.% and the 9 wt.% samples contain secondary phosphate phases with purities based on Rietveld refinement results of 93.10% and 80.40%, respectively. This indicates that 7 wt.% carbon provided a more favorable reaction condition for the conversion of ferronickel-derived $FePO_4$ into olivine $LiFePO_4$. Insufficient carbon at 5 wt.% may limit the reduction and solid-state reaction process, while excessive carbon at 9 wt.% may disturb contact between $FePO_4$ and the lithium source, leading to incomplete phase development.

Based on the morphology in Fig. 5, the 5 wt.% carbon sample consisted of large and compact agglomerates with interconnected particles, dense packing, and relatively smooth surfaces. The 7 wt.% carbon sample had a looser, more open structure. This allowed for better electrolyte access and maintained sufficient contact for electron transport. In contrast, the 9 wt.% carbon sample had a finer, more fragmented morphology. This structure might improve lithium-ion diffusion, but excessive carbon led to a non-uniform distribution and weaker contact between $LiFePO_4$ particles. BET results in Table 1 supported this interpretation. The surface area increased from 3.651 m^2/g for 5 wt.% carbon to 4.513 m^2/g for 7 wt.% carbon and 5.913 m^2/g for 9 wt.% carbon.

EIS data in Fig. 9 suggest that 7 wt.% carbon is the most favorable composition in terms of charge-transfer resistance and conductivity, while 9 wt.% carbon provides the best lithium-ion diffusion characteristics. The CV results in Fig. 10 support the EIS interpretation. The 7 wt.% carbon sample showed the highest redox peak current, indicating better electrochemical activity and faster redox kinetics. The 9 wt.% sample showed the smallest peak separation, suggesting relatively favorable lithium-ion diffusion and lower polarization. However, its lower peak current and higher charge-transfer resistance indicate that diffusion improvement alone was insufficient to deliver the best overall performance. The rate capability performance results provide direct confirmation that 7 wt.% carbon is the optimum composition in this study. The 7 wt.% sample delivered the highest specific capacity, approximately 140 mAh g^{-1} at 0.1 C, followed by 9 wt.% carbon at 113 mAh g^{-1} and 5 wt.% carbon at 68 mAh g^{-1} (Fig. 11). The higher capacity of the 7 wt.% sample can be attributed to its near-single-phase olivine structure, lower charge-transfer resistance, higher electronic conductivity, and more balanced morphology. Although the 9 wt.% sample showed the highest lithium-ion diffusion coefficient, its higher charge-transfer resistance and lower phase purity reduced its overall electrochemical performance.

Previous studies have shown that the carbon content and heat-treatment conditions have a strong impact on $LiFePO_4/C$ phase formation and electrochemical performance. The precursor crystallinity and synthesis conditions influence the electrochemical behavior of $LiFePO_4/C$ [22]. In addition, the particle size and structural state of $FePO_4$-based materials have been reported to influence reaction activity and electrochemical behavior, where nanosized particles and less crystalline structures may improve ion transport and reaction kinetics [23]. The optimal carbon content in C/LFP cathode material significantly assists in lowering the Rct and rising the Dli value in comparison with other C/LFP cathodes, but excessive carbon content increased resistance and hindered lithium-ion diffusion [24]. The residual carbon content and carbon distribution can also be affected by post heat-treatment conditions, including the duration of heat treatment [25]. This is in agreement with the present results, where the 7 wt.% carbon sample produced the highest $LiFePO_4$ phase purity and the best overall electrochemical response. However, the lower phase purity of the 9 wt.% sample shows that increasing carbon content does not always improve $LiFePO_4$ formation. In this case, excessive carbon may reduce effective contact between $FePO_4$ and the lithium source and may also cause non-uniform carbon distribution. These conditions can lead to incomplete conversion and the appearance of secondary phosphate phases.

The role of carbon observed in this work is consistent with earlier reports on the reaction mechanism of $LiFePO_4$ formation. The reduction of Fe^{3+} during $LiFePO_4$ synthesis has been reported to depend on the carbonaceous additive and thermal condition [26]. It has also been reported [27] that carbon helps maintain a reducing environment during high-temperature synthesis. These studies support the interpretation that carbon affects not only electronic conductivity, but also the local reaction environment during $LiFePO_4$ formation. In the present study, this effect was most favorable at 7 wt.% carbon, where phase conversion, electronic conductivity, and particle contact were better balanced than in the 5 wt.% and 9 wt.% samples.

The present result is also comparable with the solid-state synthesis study [28], which reported that crystalline $LiFePO_4/C$ composites could be obtained by heating pelletized precursors at 800°C for 5 h with an optimized carbon content of 3–10 wt.%. Nanocrystalline LiFePO4 particles are obtained by annealing at 550°C in Ar+5%H2 atmosphere for 3 h [29]. In this study, the optimum carbon content was 7 wt.% under different conditions, namely the use of ferronickel-derived $FePO_4$, LiOH as the lithium source, ball milling, and calcination at 650°C for 10 h under argon. This comparison shows that the optimum carbon content depends on the precursor type, carbon source, and heat-treatment route.

Compared with studies using commercial or chemically prepared $FePO_4$ precursors, the main difference in this work is the use of $FePO_4$ obtained from a ferronickel-derived solution. This is important because ferronickel-derived precursors may carry impurity risks from dissolved metal ions. The absence of detectable Ni in the final $LiFePO_4/C$ products suggests that the $FePO_4$ precipitation route was effective in reducing Ni carryover before cathode synthesis. This result supports previous findings that precursor quality and impurity control are important for improving $LiFePO_4$ cathode performance [9, 17, 30]. Therefore, the main feature of this study is not only the identification of 7 wt.% carbon as the optimum composition, but also the demonstration that ferronickel-de-

rived $FePO_4$ can be converted into $LiFePO_4$/C with promising phase purity and electrochemical performance. The applicability of these results is limited to the synthesis conditions used in this study, including the ferronickel-derived $FePO_4$ precursor, LiOH as the lithium source, Super P carbon contents of 5–9 wt.%, ball milling at 300 rpm for 2 h, preheating at 300°C for 3 h, and calcination at 650°C for 10 h under an argon atmosphere. The optimum 7 wt.% carbon value cannot be generalized to other lithium sources, carbon sources, furnace atmospheres, or heat-treatment temperatures without further verification.

The obtained capacity remains below the theoretical 170 mAh g^{-1} of $LiFePO_4$, but the result is promising because the precursor was derived from ferronickel, not high-purity commercial $FePO_4$. The gap between experimental and theoretical capacity may be due to particle agglomeration, incomplete carbon coating, limited active material utilization, and non-optimized particle size distribution.

From a practical point of view, the results of this study show that ferronickel-derived $FePO_4$ has potential to be used as an alternative precursor for $LiFePO_4$/C cathode materials. The findings are mainly applicable to the early development of battery cathode materials using iron resources obtained from ferronickel processing. In this context, the study provides useful information for selecting the appropriate carbon content when non-commercial $FePO_4$ is used as the starting material.

The main disadvantages of this study are related to particle agglomeration, incomplete carbon coating, and the limited optimization of particle size and carbon distribution. The future development of this study will focus on the problem of particle agglomeration and incomplete carbon coating. This is possible through the variation of the carbon source and also modification of parameters in the synthesis process. The source of $FePO_4$ from ferronickel is promising because no Ni signal was detected within the detection limit of EDX analysis in the final $LiFePO_4$/C products. Therefore, the present result supports the feasibility of using ferronickel-derived $FePO_4$ as an alternative precursor, provided that impurity control is maintained during precursor preparation. However, for the future development may have a several experimental difficulties, especially in maintaining consistent $FePO_4$ precursor purity from ferronickel-derived solutions, controlling residual metal impurities, and achieving uniform carbon distribution during larger-scale synthesis. Further optimization should include precursor reproducibility, carbon-coating characterization, and long-term cycling stability tests.

7. Conclusions

1. The carbon addition significantly affected the formation of the olivine $LiFePO_4$ phase and secondary phase development. The 7 wt.% sample showed an LFP peak and reached 99.60% purity. In contrast, the 5 wt.% and 9 wt.% samples contained secondary phosphate phases with purities of 93.10% and 80.40%, respectively. This suggests that 7 wt.% carbon provided a more favorable reaction condition for converting ferronickel-derived $FePO_4$ into olivine $LiFePO_4$.

2. The effect of carbon addition on the microstructural characteristics of $LiFePO_4$/C materials concludes that carbon coating can reduce the agglomeration of the LFP particles. The lack of carbon coating tends to produce agglomerates and growth of particles becomes dense; this is shown in samples with 5 wt.%. The 7 wt.% carbon sample had a less compact particle structure, with a looser structure that allowed better electrolyte access and maintained electron transport. The 9 wt.% carbon sample had a finer, more fragmented morphology.

3. Among the synthesized materials, adsorption uptake increases with increasing carbon content, which is 9 wt.%, 7 wt.%, and 5 wt.% in sequence. Although higher carbon content increased the adsorption uptake and BET surface area, the electrochemical results show that textural improvement alone was insufficient to achieve superior cathode performance.

4. The electrochemical performance of $LiFePO_4$/C cathodes, based on CV, EIS, and galvanostatic charge–discharge tests, confirms that 7 wt.% carbon is the optimum composition in this study. The 7 wt.% sample delivered the highest specific capacity, approximately 140 mAh g^{-1} at 0.1 C, followed by 9 wt.% carbon at 113 mAh g^{-1} and 5 wt.% carbon at 68 mAh g^{-1}. The 7 wt.% sample is lower charge-transfer resistance and higher electronic conductivity. Although the 9 wt.% sample showed the highest lithium-ion diffusion coefficient, its higher charge-transfer resistance and lower phase purity reduced its overall electrochemical performance.

Conflict of interest

The authors declare that they have no conflict of interest in relation to this study, whether financial, personal, authorship or otherwise, that could affect the study and its results presented in this paper.

Financing

This work was conducted as part of the first author's doctoral study supported by Beasiswa Pendidikan Indonesia (BPI), under the Ministry of Higher Education, Science, and Technology of the Republic of Indonesia.

Data availability

Data will be made available on reasonable request.

Use of artificial intelligence

The authors confirm that no generative artificial intelligence tools were used to create scientific content, generate data, perform analysis, or draw conclusions in this work.

Acknowledgment

The authors would also like to thank PT ANTAM Tbk. For providing the FeNi material.

Authors' contributions

Vita Astini: Conceptualization, **Methodology,** Validation**, Formal analysis,** Investigation, **Writing – original draft**, **Writing – review & editing; Anne Zulfia Syahrial: Conceptualization**, **Resources**, **Supervision; Ahmad Subhan:** Conceptualization, Supervision**; Johny Wahyuadi M. S:** Conceptualization, Supervision

References

1. Mohamed, N., Allam, N. K. (2020). Recent advances in the design of cathode materials for Li-ion batteries. RSC Advances, 10 (37), 21662–21685. https://doi.org/10.1039/d0ra03314f
2. Seher, J., Fröba, M. (2021). Shape Matters: The Effect of Particle Morphology on the Fast-Charging Performance of $LiFePO_4$/C Nanoparticle Composite Electrodes. ACS Omega, 6 (37), 24062–24069. https://doi.org/10.1021/acsomega.1c03432
3. Lara, C., Maril, M., Tobosque, P., Núñez, J., Pizarro, L., Carrasco, C. (2025). Comprehensive analysis of improved LiFePO4 kinetics: Understanding barriers to fast charging. Journal of Power Sources, 640, 236747. https://doi.org/10.1016/j.jpowsour.2025.236747
4. Kaur, G., Gates, B. D. (2022). Review – Surface Coatings for Cathodes in Lithium Ion Batteries: From Crystal Structures to Electrochemical Performance. Journal of the Electrochemical Society, 169 (4), 43504. https://doi.org/10.1149/1945-7111/ac60f3
5. Chen, S.-P., Lv, D., Chen, J., Zhang, Y.-H., Shi, F.-N. (2022). Review on Defects and Modification Methods of LiFePO4 Cathode Material for Lithium-Ion Batteries. Energy & Fuels, 36 (3), 1232–1251. https://doi.org/10.1021/acs.energyfuels.1c03757
6. Kang, H., Wang, G., Guo, H., Chen, M., Luo, C., Yan, K. (2012). Facile Synthesis and Electrochemical Performance of $LiFePO_4$/C Composites Using Fe–P Waste Slag. Industrial & Engineering Chemistry Research, 51 (23), 7923–7931. https://doi.org/10.1021/ie300088p
7. Kumar, K., Kumar, S., Sen, A., Mediboyana, H., Bag, S. S., Kundu, R. (2024). Utilizing Cold Rolling Mill Iron Oxide To Synthesize Lithium Iron Phosphate for Li-Ion Batteries. ACS Sustainable Resource Management, 1 (6), 1185–1194. https://doi.org/10.1021/acssusresmgt.4c00065
8. Khalil, S. B., Broughel, A. (2025). Stainless success, battery lag: Evaluation of Indonesia's resource nationalism in nickel. The Extractive Industries and Society, 23, 101677. https://doi.org/10.1016/j.exis.2025.101677
9. Jeong, T., Mohanty, S. K., Kwon, W. J., Reddy, S. C., Pati, A. R., Ryu, J. H., Yoo, H. D. (2025). Tailoring iron phosphate precursors via microcrystallization for high-performance lithium iron phosphate cathodes in lithium-ion batteries. Journal of Materials Chemistry A, 13 (22), 16694–16703. https://doi.org/10.1039/d5ta00679a
10. Yuan, Y., Hu, J., Wang, L., Li, Y., Yao, Y. (2024). Structural properties and electrochemical performance of different polymorphs of $FePO_4$ as raw materials for lithium ion electrodes. Journal of Materials Chemistry C, 12 (18), 6511–6518. https://doi.org/10.1039/d4tc00957f
11. Song, Y., Fu, Z. (2024). Mini-Review on the Preparation of Iron Phosphate for Batteries. Energy & Fuels, 38 (19), 18194–18207. https://doi.org/10.1021/acs.energyfuels.4c02533
12. Shen, Z.-Z., Wang, R.-X., Yuan, H.-Y., Guo, Y., Xiao, D., Meng, Y. (2025). Waste to treasure: A sustainable technic to prepare high-performance lithium iron phosphate from laterite nickel tailings. Separation and Purification Technology, 353, 128489. https://doi.org/10.1016/j.seppur.2024.128489
13. Chang, L., Wei, A., Luo, S., Bi, X., Yang, W., Yang, R., Liu, J. (2023). Preparation of LiFePO4/C cathode material by extracting Fe_2O_3 from laterite nickel ore by ammonium jarosite method. Journal of Alloys and Compounds, 936, 168078. https://doi.org/10.1016/j.jallcom.2022.168078
14. Ishtiaq, S., Majid, A., Qadeer, A., Alkhedher, M., Bulut, N. (2025). Recent progress in carbon coating and surface modification of LiFePO4 cathodes. RSC Advances, 15 (50), 42331–42346. https://doi.org/10.1039/d5ra05833c
15. Yuan, Y., Zhou, W., Dai, X., Wu, F., Chen, H., Mai, Y. et al. (2025). Regulation of nano FePO precursors and exploration of influencing mechanisms in LiFePO4/C cathode. New Journal of Chemistry, 49 (5), 1802–1813. https://doi.org/10.1039/d4nj04412f
16. Zhi, X., Liang, G., Wang, L., Ou, X., Gao, L., Jie, X. (2010). Optimization of carbon coatings on LiFePO4: Carbonization temperature and carbon content. Journal of Alloys and Compounds, 503 (2), 370–374. https://doi.org/10.1016/j.jallcom.2010.02.173
17. Ma, G., Luo, X., Cheng, M., Ju, D. (2025). Effect of impurities in FePO4 raw materials on the performance of $LiFePO_4$ cathode materials. Scientific Reports, 15 (1). https://doi.org/10.1038/s41598-025-99729-8
18. Syahrial, A. Z., Astini, V., M.S, J. W. (2025). Electrolysis and precipitation-based purification of ferronickel for high-purity nickel production. Eastern-European Journal of Enterprise Technologies, 3 (6 (135)), 46–53. https://doi.org/10.15587/1729-4061.2025.324608
19. Astini, V., Meirawati, S., Nengsih, S., -, A., -, H., Soedarsono, J. W. M., Zulfia, A. (2024). Influence of Electrolyte Molarity and Applied Voltage on the Purification of Ferronickel by Electrolysis Method. Metalurgi, 39 (1), 7. https://doi.org/10.55981/metalurgi.2024.742
20. Kashi, R., Khosravi, M., Mollazadeh, M. (2018). Effect of carbon precursor on electrochemical performance of LiFePO4-C nano composite synthesized by ultrasonic spray pyrolysis as cathode active material for Li ion battery. Materials Chemistry and Physics, 203, 319–332. https://doi.org/10.1016/j.matchemphys.2017.10.021
21. Li, B., Xiao, J., Zhu, X., Wu, Z., Zhang, X., Han, Y. et al. (2024). Enabling high-performance lithium iron phosphate cathodes through an interconnected carbon network for practical and high-energy lithium-ion batteries. Journal of Colloid and Interface Science, 653, 942–948. https://doi.org/10.1016/j.jcis.2023.09.133
22. Zhang, T., Lin, S., Yu, J. (2022). Influence Mechanism of Precursor Crystallinity on Electrochemical Performance of $LiFePO_4$/C Cathode Material. Industrial & Engineering Chemistry Research, 61 (15), 5181–5190. https://doi.org/10.1021/acs.iecr.1c04784
23. Zhang, S. M., Zhang, J. X., Xu, S. J., Yuan, X. J., Tian, T. (2013). Synthesis of Nano-Sized FePO4 Cathode Material via a Microemulsion Technique. Applied Mechanics and Materials, 320, 675–682. https://doi.org/10.4028/www.scientific.net/amm.320.675

24. Hsieh, C.-T., Pai, C.-T., Chen, Y.-F., Chen, I.-L., Chen, W.-Y. (2014). Preparation of lithium iron phosphate cathode materials with different carbon contents using glucose additive for Li-ion batteries. Journal of the Taiwan Institute of Chemical Engineers, 45 (4), 1501–1508. https://doi.org/10.1016/j.jtice.2013.12.017
25. Rajoba, S. J., Jadhav, L. D., Kalubarme, R. S., Yadav, S. N. (2019). Influence of synthesis parameters on the physicochemical and electrochemical properties of LiFePO4 for Li-ion battery. Journal of Alloys and Compounds, 774, 841–847. https://doi.org/10.1016/j.jallcom.2018.09.325
26. Ravet, N., Gauthier, M., Zaghib, K., Goodenough, Mauger, A., Gendron, F. (2007). Mechanism of the Fe3+ Reduction at Low Temperature for LiFePO4 Synthesis from a Polymeric Additive. Chemistry of Materials, 19 (10), 2595–2602. https://doi.org/10.1021/cm070485r
27. Feng, H., Milev, A. S., Kannangara, G. S. K. (2014). Novel Co-Precipitation Method for Synthesis of Carbon-Free LiFePO4. ECS Meeting Abstracts, MA2014-01 (2), 250. https://doi.org/10.1149/ma2014-01/2/250
28. Zhang, S. S., Allen, J. L., Xu, K., Jow, T. R. (2005). Optimization of reaction condition for solid-state synthesis of LiFePO4-C composite cathodes. Journal of Power Sources, 147 (1-2), 234–240. https://doi.org/10.1016/j.jpowsour.2005.01.004
29. Scaccia, S., Carewska, M., Wisniewski, P., Prosini, P. P. (2003). Morphological investigation of sub-micron FePO4 and LiFePO4 particles for rechargeable lithium batteries. Materials Research Bulletin, 38 (7), 1155–1163. https://doi.org/10.1016/s0025-5408(03)00110-7
30. Dadwal, K., Fábián, M., Tolnai, I., Sharma, S., Kaur, R., Gracheva, M. et al. (2025). Neutron, X-ray diffraction, DSC, Raman, Mössbauer and leaching studies of iron phosphate glasses and crystalline phases. RSC Advances, 15 (7), 5286–5304. https://doi.org/10.1039/d5ra00295h